

CHEMICAL ABUNDANCES OF PLANETARY NEBULAE IN M31

GEORGE H. JACOBY

Kitt Peak National Observatory, National Optical Astronomy Observatories¹

AND

HOLLAND C. FORD²

Space Telescope Science Institute

Received 1984 October 9; accepted 1985 August 30

ABSTRACT

We have measured chemical abundances in M31's disk and halo by observing three planetary nebulae and an H II region at projected distances of 3.5, 18 and 33 kpc. We used a direct measurement of the temperature in the H II region BA 685 to validate the empirical temperature, O/H, and N/H scales derived by Dennefeld and Kunth and by Blair, Kirshner, and Chevalier. Our measurements of O/H in a disk planetary nebula and H II region show that abundances are high in M31's interstellar medium in comparison with the Galaxy, and that there has been little enrichment since the birth of the planetary nebula progenitors at $t \geq 2 \times 10^9$ yr ago. In spite of the fact that the present star formation rate in M31 is lower than in the Galaxy, and quite low at $R = 18$ kpc, the abundances in M31 at $R = 18$ kpc are similar to those in the Orion nebula. These data show that M31 experienced considerably more enrichment of its interstellar medium during its early life than did the Galaxy.

Kinematical considerations show that M31-290 and M31-372 belong to a halo population similar to that of M31's globular clusters. Comparison of the oxygen abundances in the two halo planetaries provides direct evidence for the chemical heterogeneity in M31's halo deduced from measurements of the integrated line strengths of globular clusters. We conclude that, in contrast to the Galaxy, there is little evidence for a relationship between kinematics and metallicity in the halo of M31. The evidence suggests that a wide range of metal enrichment occurred during the collapse of M31's halo, with only weak, progressive enrichment toward its center.

Subject headings: galaxies: individual — interstellar: abundances — nebulae: abundances — nebulae: H II regions — nebulae: planetary

I. INTRODUCTION

Planetary nebulae in nearby galaxies serve as probes of the chemical composition of the older stellar populations. Presently they provide the only means for measuring chemical abundances in individual stars at the distance of M31. An abundance study based on disk planetary nebulae along M31's major axis will reveal even a small abundance gradient over a sufficiently long baseline. Furthermore, comparison of abundances in planetary nebulae with abundances in H II regions (Blair, Kirshner, and Chevalier 1982) and supernova remnants (Blair, Kirshner, and Chevalier 1981, 1982) provides a measure of the enrichment of the interstellar medium during the interval between the birth of the planetary nebula progenitors and the present.

Thus far there have been chemical composition measurements for planetary nebulae in NGC 6822 (Dufour and Talent 1980), Fornax (Danziger *et al.* 1978), NGC 185 (Jenner and Ford 1978; Ford 1983), M32 (Jenner, Ford, and Jacoby 1979), and the Magellanic Clouds (Osmer 1976; Dufour and Killen 1977; Aller *et al.* 1981; and Aller 1983). Those abundances, including preliminary results for planetary nebulae in M31, were reviewed by Ford (1983). In this paper we present detailed results for three planetary nebulae at projected distances of 3.5, 18, and 33 kpc from the center of M31, and, for comparison, an

H II region 17 kpc from the center. We then compare the kinematics and abundances of the nebulae to globular clusters in M31 and discuss the history of chemical enrichment in M31's disk and halo.

II. OBSERVATIONS

a) *A Survey for Distant Disk and Halo Planetary Nebulae*

We must sample the distribution of planetary nebula abundances over a wide range of distances from the center of M31 in order to measure small composition gradients. This requires a selection of planetary nebulae along the major axis of M31 extending to distances greater than 20 kpc. To accomplish this, we used pairs of [O III] $\lambda 5007$ on-line and off-line plates taken at the prime focus of the Kitt Peak Mayall 4 m telescope to identify planetary nebulae in fields along M31's northeast and southwest major axes. The fields extended along the major axis from 16 to 49 kpc on the northeast side and from 14 to 36 kpc on the southwest side. We subsequently used spectrophotometric radial velocity scans taken with the Kitt Peak intensified image dissector scanner (IIDS) on the 4 m telescope to confirm that 33 of the 41 candidate nebulae are indeed planetary nebulae in M31. One of the remaining eight candidates was a faint, semi-stellar H II region (BA 685, Baade and Arp 1964); the other seven faint candidates could not be found with the IIDS.

We supplemented the prime focus survey on the northeast side of M31 with [O III] $\lambda 5007$ interference filter on-line and off-line plate pairs taken with a Carnegie image tube camera

¹ Operated by the Association of Universities for Research in Astronomy, Inc., under contract with the National Science Foundation.

² Visiting Observer, Kitt Peak National Observatory.

TABLE 1
SURVEYS AND POSITIONS FOR NEBULAE IN M31

OBJECT	SURVEY				POSITION (1975.0)	
	Telescope	Plate	Filter	Exposure (minutes)	R.A.	Decl.
M31-290 ^a	Shane 3 m	II a-D	5007/50	45	00 ^h 42 ^m 14 ^s .80	41°22'53".2
M31-363 ^a	Mayall 4 m	IIIa-J	5012/32	150	00 45 36.23	42 29 47.0
BA 685	Mayall 4 m	IIIa-J	5012/32	150	00 45 26.86	42 19 30.0
M31-372 ^a	Kitt Peak No. 1 0.9 m	IIIa-J	5009/22	40	00 45 18.25	43 50 52.7

on the Kitt Peak No. 1 0.9 m telescope. We surveyed a region adjacent to and on the northwest side of our prime focus fields in an area which appears to follow the warp of M31's disk (Innanen *et al.* 1982). As anticipated, we found several (eight) additional faint nebulae at large projected distances from M31's center. The results of the surveys and radial velocity observations will be presented in detail in another paper (Nolthenius and Ford 1986).

We chose two planetary nebulae from these surveys for our abundance study. The first, M31-372, was found in the image tube survey and has a projected distance of 33 kpc, which is the largest distance in our sample. The second nebula, M31-363, has a projected distance of 18 kpc. In order to make a direct comparison between abundances in old and young stars at this distance, we also observed the H II region BA 685, which has $R_{\text{projected}} = 17$ kpc and appears on our plates as a slightly resolved nebula that is noticeably brighter than the planetaries. Finally, in order to have a long baseline, we observed the planetary nebula M31-290 (Ford and Jacoby 1978a), which has $R_{\text{projected}} = 3.5$ kpc (the projected distance was erroneously given as 10 kpc in Ford 1983). The kinematic properties and population assignments of the nebulae are discussed in § IV. The projected positions of the nebulae relative to M31 are shown schematically in Figure 1 (Plate 8). Finding charts for M31-372 and M31-363 are given in Figure 2 (Plate 9). A summary of the photographic survey is given in Table 1.

b) Spectroscopy

The key parameter in an abundance analysis of emission line objects is the plasma electron temperature. In the optical, the best temperature diagnostic for high-excitation planetary nebulae such as these is the ratio of the [O III] lines ($I(\lambda 4363)/I(\lambda 5007)$). This ratio is generally on the order of 0.01 for temperatures near 10,000 K. This corresponds to an equivalent broad-band magnitude of ~ 25.5 in the $\lambda 4363$ line for bright planetary nebulae in M31. The observational difficulties are

further exacerbated by the proximity of the city-glow mercury emission line at 4358 Å. In spite of these difficulties, the temperature can be measured with very long integration times, but the number of nebulae is necessarily limited to one or two per night.

We obtained spectra during two observing runs in 1981 and 1982 as summarized in Table 2, using the Kitt Peak Mayall 4 m telescope and the IIDS. Spectra extending from 3550 to 6900 Å were taken using two spectrograph configurations. A blue setup using a 600 line grating (No. 26) in first order provided coverage from 3550 to 5350 Å. A red setup consisting of a 500 line grating (No. 240), also used in first order with a Schott GG-420 order separation filter, provided coverage from 4800 to 6900 Å. The resulting spectral resolutions in the blue and red are 7 and 8 Å respectively.

All observations were taken in the "beam-switch" mode, whereby the object is placed first in one aperture for 4 minutes while the other aperture samples the sky spectrum, and then the procedure is reversed. The entrance apertures used have a diameter of 3".2 and a separation of 52". Seeing was generally very good, on the order of 1"–1".5, so that the derived absolute fluxes are likely to be accurate. Care was taken to avoid observations at large airmasses to minimize systematic errors arising from atmospheric dispersion, especially in the blue spectral region.

c) Reductions

The data were reduced according to the usual procedures for scanner data. High-frequency pixel-to-pixel variations were removed by dividing all object spectra by the spectrum of a continuum lamp. The spectra were then placed on a linear wavelength scale using the pixel-to-wavelength mapping function derived from observations of a lamp producing emission lines of helium, neon, and argon. This comparison lamp was observed every time the telescope was moved to a new object in order to minimize the effects of flexure. The raw counts were then corrected for atmospheric extinction using mean extinction coefficients for Kitt Peak. Data from the two apertures were combined to remove the sky and underlying galaxy continuum contributions and corrected for the instrumental sensitivity variations through nightly observations of flux standards. In some instances, the spectra from successive nights were added together to form a grand average (e.g., M31-372 at 33 kpc). The resulting blue and red spectra for the three planetary nebulae and the H II region are shown in Figures 3–6.

The fluxes of the important emission lines relative to the flux 5007 Å are computed independently for the blue and red spectral regions. The relative fluxes across the spectrum are then tied together through the strongest line in the spectrum. It is worth noting that the differences between the absolute fluxes

TABLE 2
JOURNAL OF SPECTROSCOPIC OBSERVATIONS

Object	Spectral Region	Date	Exposure (minutes)
M31-290	Blue	1981 Oct 25/26	224
	Red	1981 Oct 25/26	56
M31-363	Blue	1982 Nov 4/5	240
	Red	1982 Nov 3/4	104
BA 685	Blue	1982 Nov 4/5	72
	Red	1982 Nov 3/4	32
M31-372	Blue	1981 Oct 23/24–24/25	400
	Red	1981 Oct 24/25	64

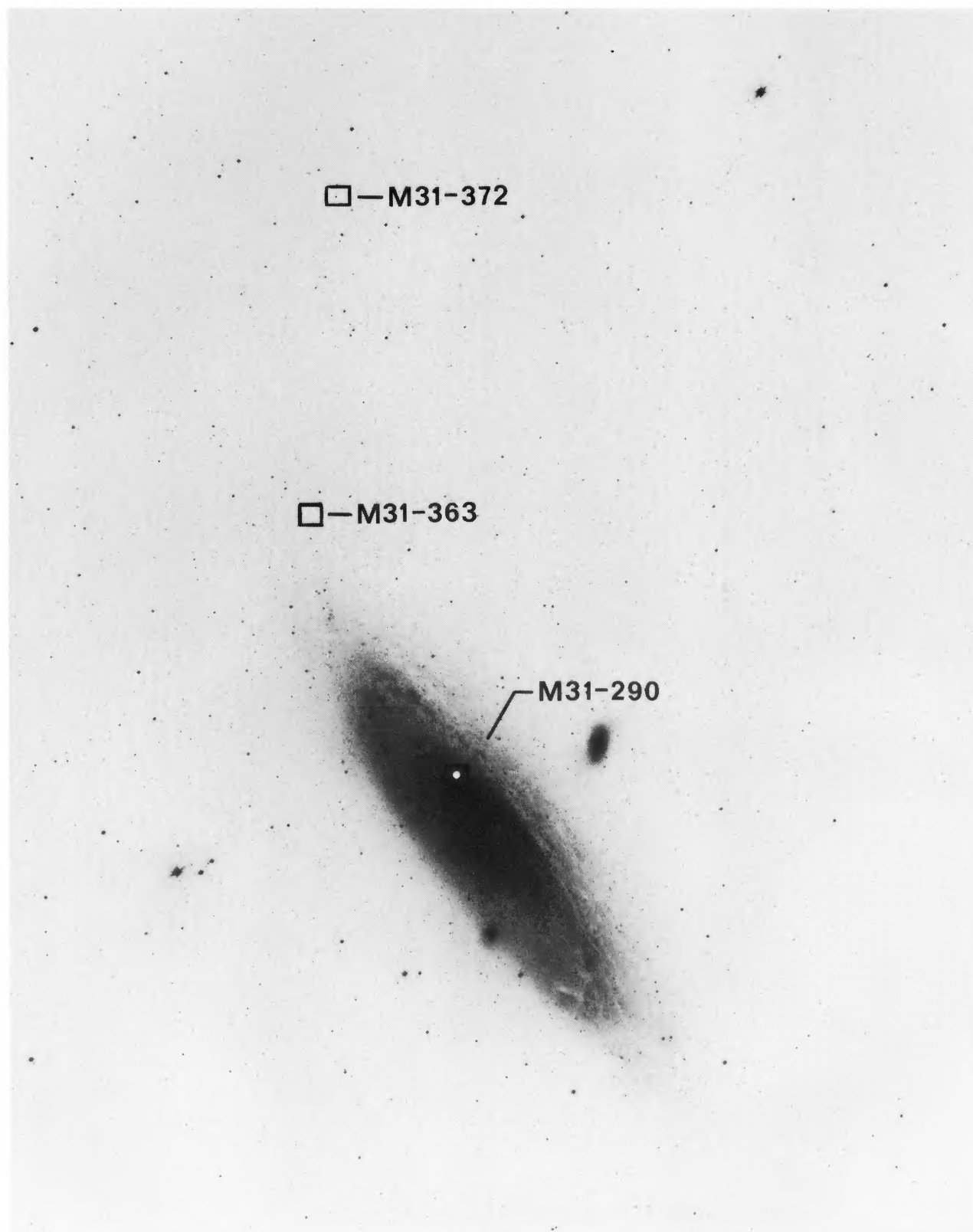
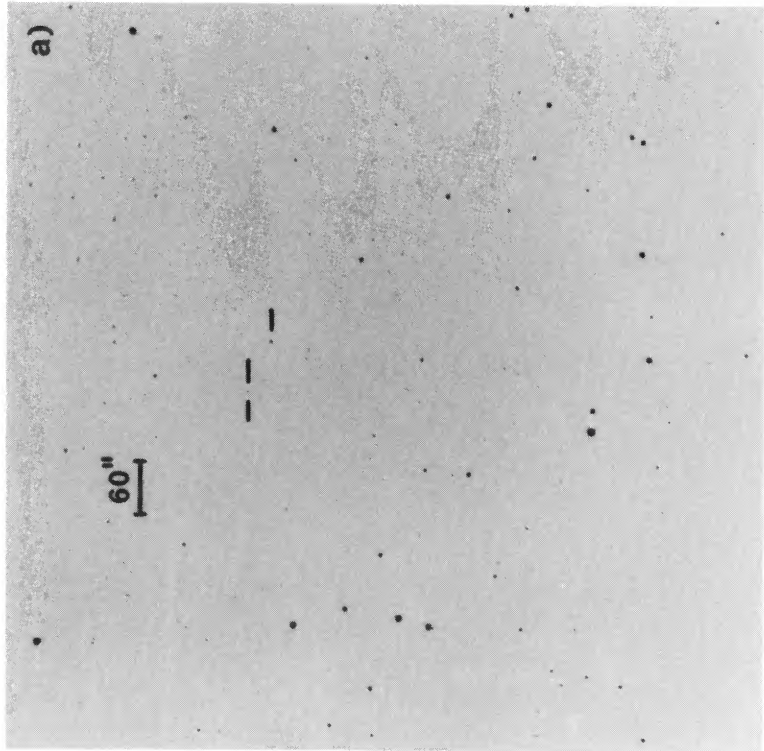


FIG. 1.—Locations of the three planetary nebulae (M31-290, M31-363, and M31-372); reproduction of Palomar Observatory Sky Survey red plate

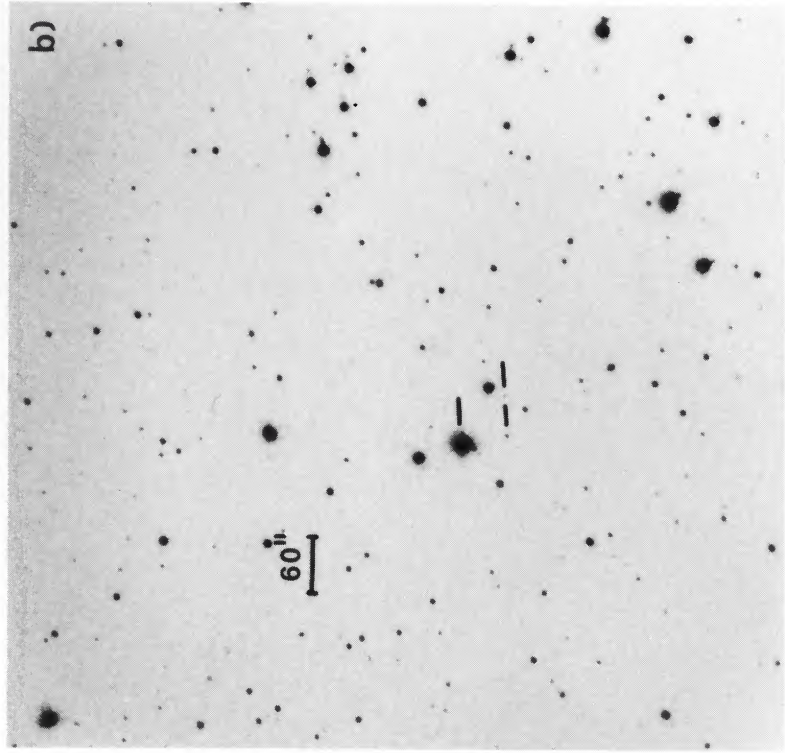
JACOBY AND FORD (*see* page 491)

N



M31-363

E



M31-372

FIG. 2.—(a) Finding chart for nebula M31-363. Single line marks a positional reference star having coordinates $\alpha_{1975} = 00^{\text{h}}45^{\text{m}}31^{\text{s}}.26$, $\delta_{1975} = 42^{\circ}29'19''.7$. (b) Finding chart for nebula M31-372. Positional reference star is at $\alpha_{1975} = 00^{\text{h}}45^{\text{m}}22^{\text{s}}.75$, $\delta_{1975} = 43^{\circ}51'32''.1$.

JACOBY AND FORD (see page 491)

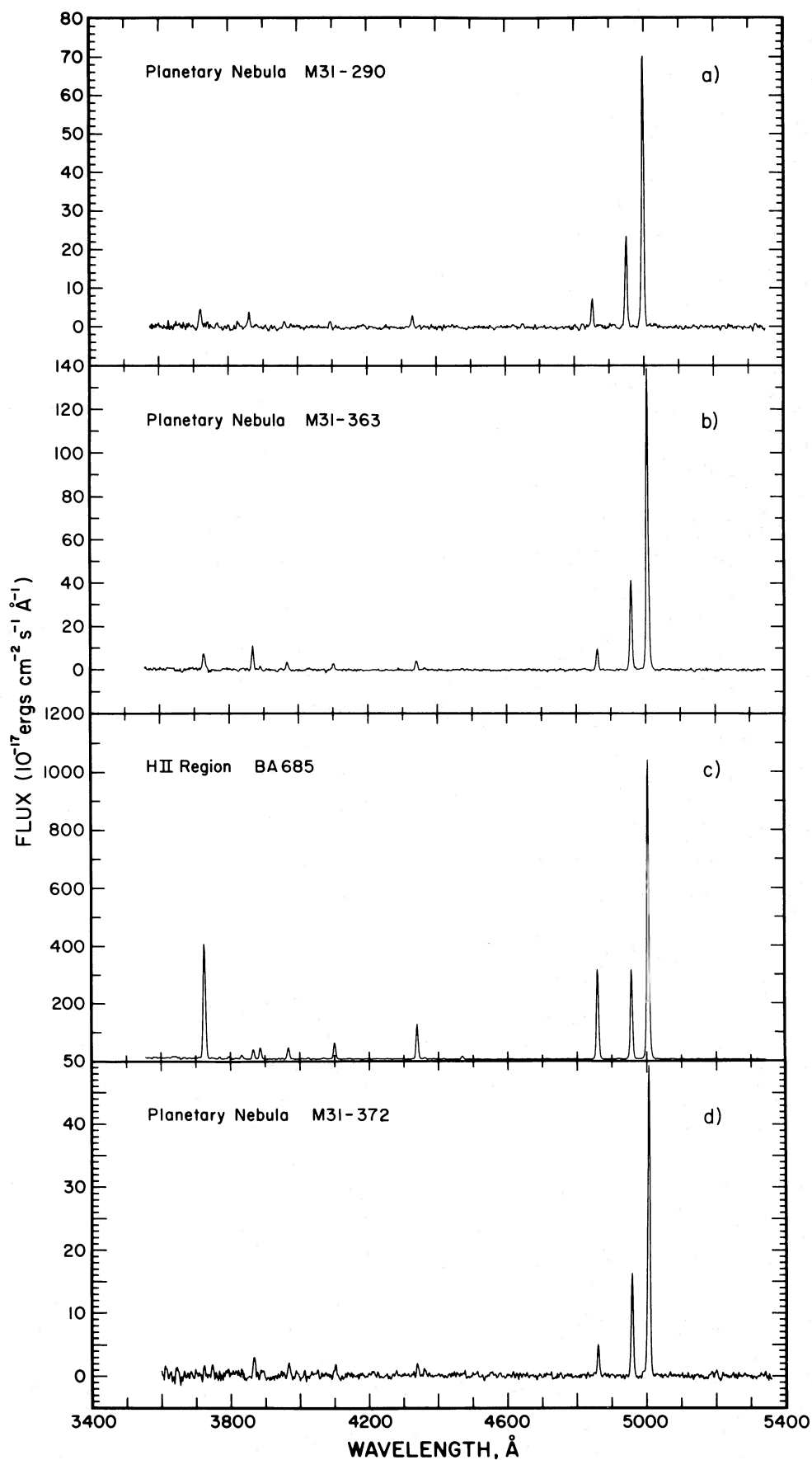


FIG. 3.—Spectra for the four nebulae in the blue spectral region

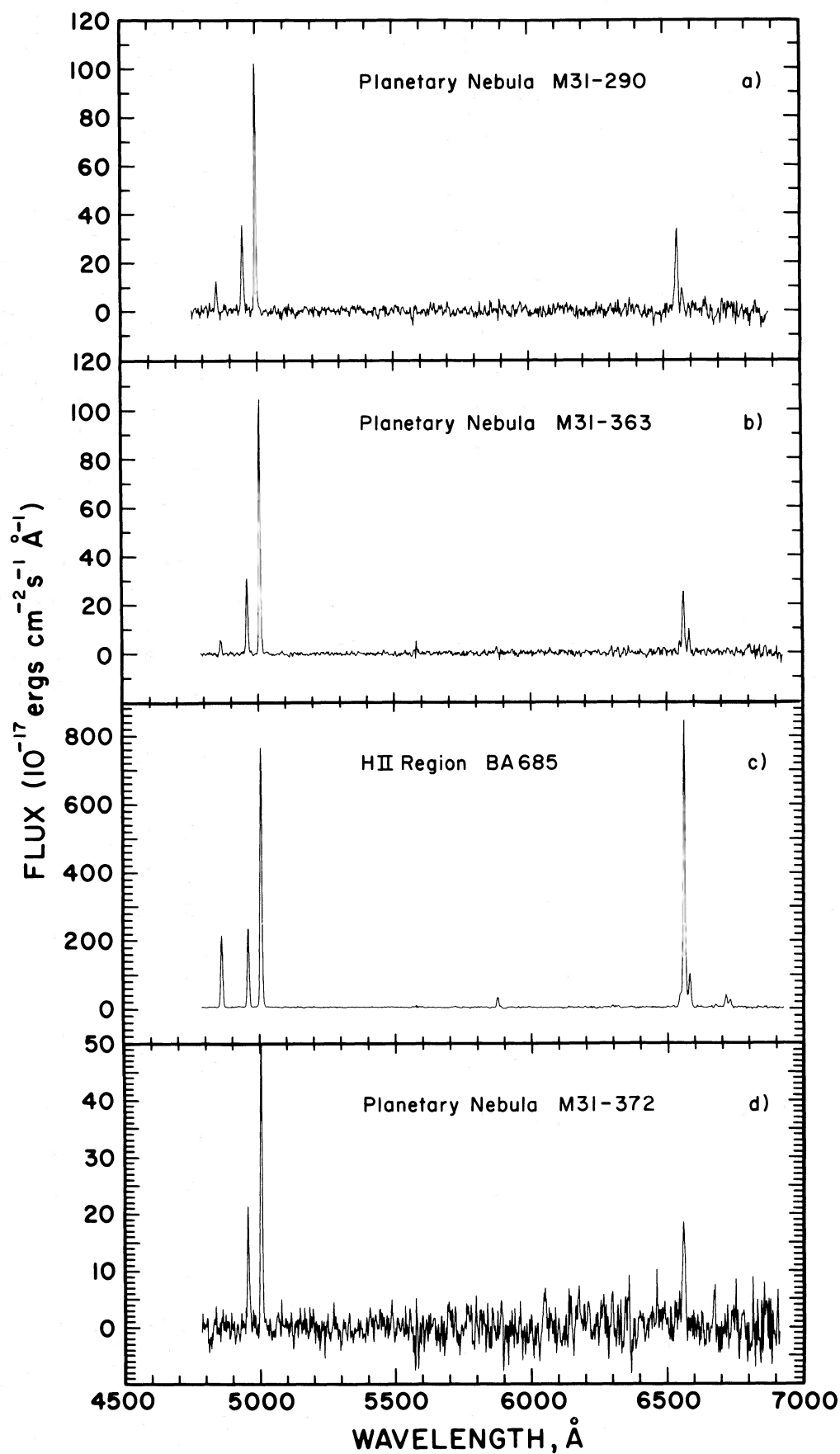


FIG. 4.—Spectra for the four nebulae in the red spectral region

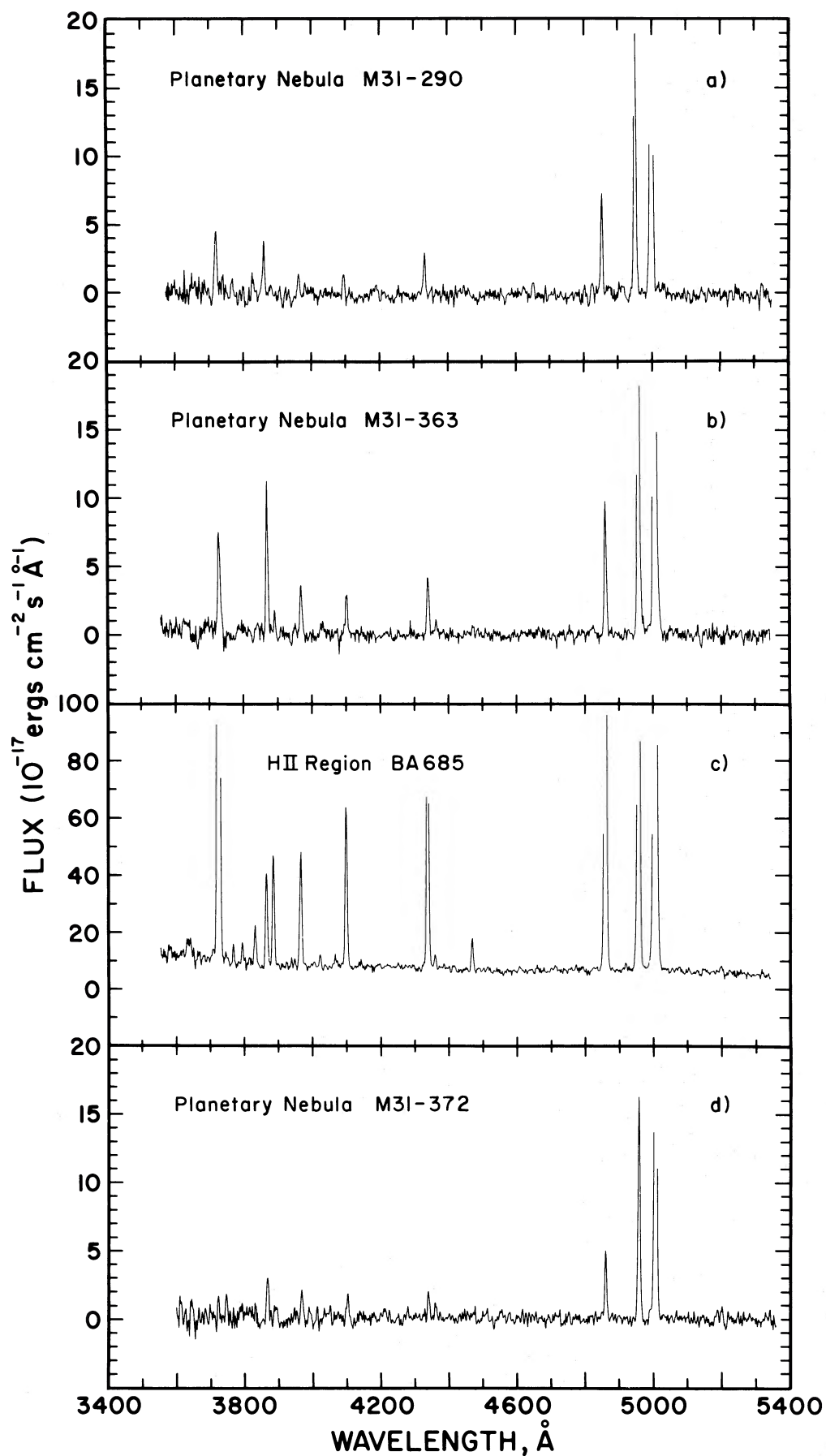


FIG. 5.—Same as Fig. 3, but expanded vertically to show the weaker lines. Horizontal scale identical to that in Fig. 3.

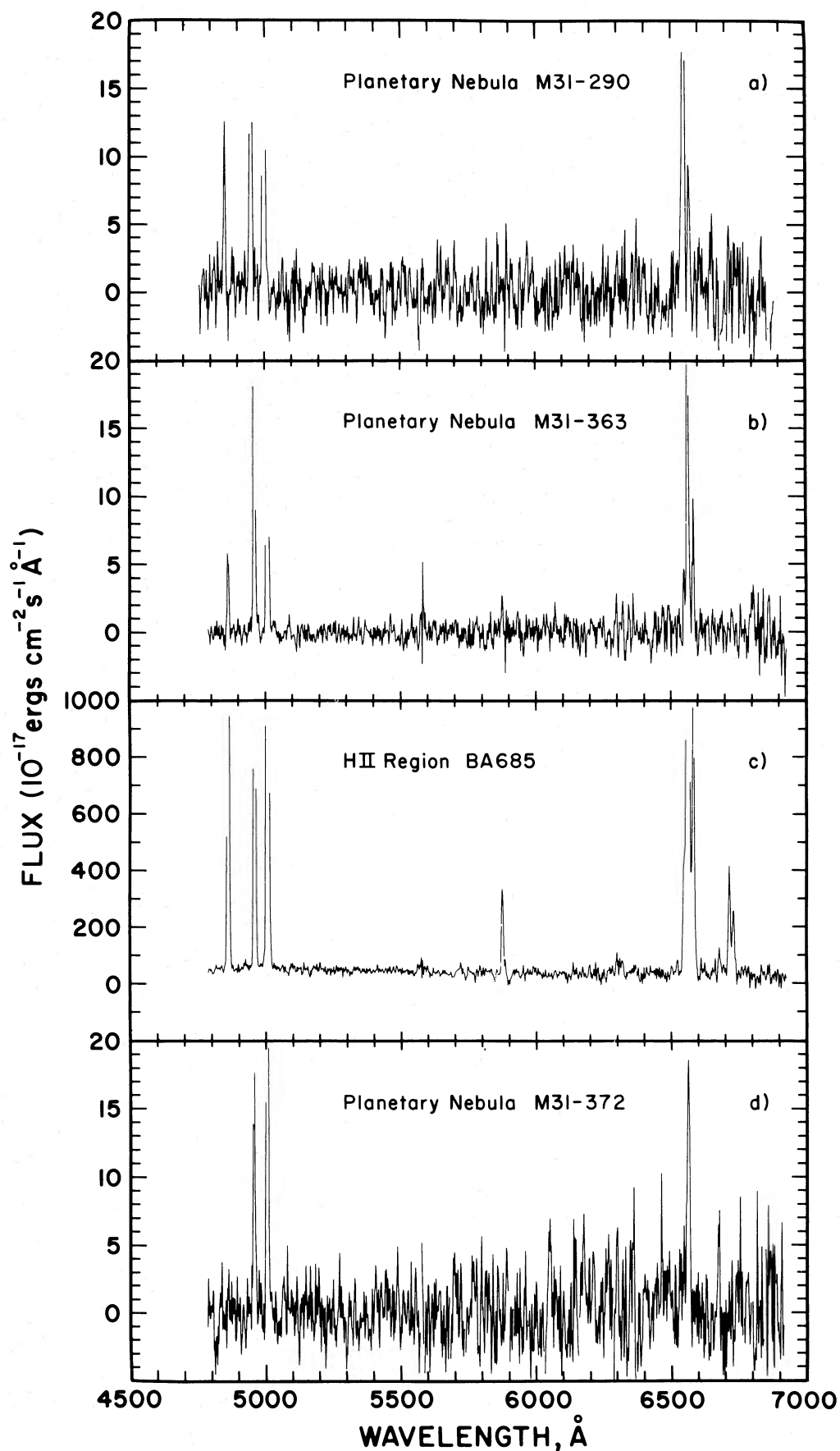


FIG. 6.—Same as Fig. 4, but expanded vertically to show the weaker lines. Horizontal scale identical to that in Fig. 4.

for 5007 Å are typically smaller than 10% as measured from the two spectral regions. The relative line strengths for the four nebulae are given in Table 3.

Because the lines of H α and [N II] $\lambda\lambda$ 6548, 6583 are partially blended, a deconvolution procedure was employed to extract the intensities of the individual components. The three lines were represented by Gaussian distributions having the same width. The three distributions are constrained to be separated by their difference in wavelengths, but the position of the group is free to shift in order to allow for the object's redshift. A nonlinear least-squares fit to the data yields the redshift, the Gaussian width, and the relative intensities of the three lines. The results of the deconvolution were used to derive the relative line strengths listed in Table 3 for these three lines. The same technique was used for the [S II] $\lambda\lambda$ 6717, 6731 lines in the H II region.

We used the ratios of the Balmer lines to determine the interstellar reddening along the line of sight. The adopted dereddened ratio of H α /H β /H γ is 2.85/1.00/0.469 (Brocklehurst 1971). For some of the observations, the two line ratios yielded slightly different values for the logarithmic extinction at H β . In those cases, we took the value derived from the ratio of H α /H β because of the greater signal-to-noise ratio in this pair of lines. Values for the reddening parameter c , the reddening function f_λ derived from Whitford (1958), the dereddened line intensities relative to H β , and line quality estimates are given in Table 3. Also included are the observed fluxes for H β .

We derived the line quality estimates in the following way. All spectra for each object were co-added to form sums of object plus sky, sky, and the difference (object sum minus sky sum). The total counts contributing to each emission line were measured by integrating the spectrum under the line, or by deconvolution in the case of the H α + [N II] and [S II] complexes. For the weaker lines, the signal-to-noise ratio is dominated not by the photon noise in the emission line, but rather by

the underlying sky continuum and occasional emission lines. The sky contributions were computed by measuring the average sky level at the wavelength of the emission lines of interest and multiplying by twice the full-width at half maximum (FWHM) of the emission line. This approximates the total count integral under the measured emission line.

Counts are then converted to photons using the approximation that for the IIDS, one count represents 1.5 photons, as suggested by Goad (1979). The signal-to-noise ratio is then $SNR = N_l/(N_l + 2N_s)^{1/2}$, where N_l is the photon count in the emission line and N_s is the photon count in the underlying sky. Note that the sky contribution enters twice: once due to the object plus sky sum, and again during the subtraction process to remove the (independent) sky spectrum. This suggests that an improvement of up to a factor of $2^{1/2}$ can be realized by not subtracting the sky spectrum; but then the structure in the sky spectrum complicates measurement of the emission lines and can introduce systematic errors.

The reddening values in Table 3 yield color excesses $E(B-V)$ which increase from 0.25 to 0.55 as the distance from the center increases from 3.5 to 31 kpc. A more typical value for M31 is 0.11 (McClure and Racine 1969). The difference suggests an increase in dust along the line of sight as we move outward along the northeast major axis of M31. Note that when the H β fluxes in Table 3 are corrected for the calculated extinction, all three planetary nebulae have the same flux to within 5%. This is the expected result from selecting the brightest nebulae, and from the empirical observation that planetary nebulae have an upper brightness limit (Jacoby and Lesser 1981).

III. ABUNDANCES

The ionic concentrations relative to hydrogen are sensitive to both electron density and temperature. The density is best calculated from the ratios of the [O II] and [S II] doublets

TABLE 3
DEREDDENED LINE STRENGTHS RELATIVE TO H β AND QUALITY INDICES^a

Wavelength (Å)	Ion	f_λ	M31-290		M31-363		BA 685		M31-372	
			I_λ	QI	I_λ	QI	I_λ	QI	I_λ	QI
3727	[O II]	+0.315	0.852	<i>b</i>	1.476	<i>a</i>	1.973	<i>a</i>	0.354	<i>d</i>
3869	[Ne III]	+0.270	0.549	<i>b</i>	1.420	<i>a</i>	0.138	<i>a</i>	1.343	<i>b</i>
3969	[Ne III] + H7	+0.235	0.235	<i>c</i>	0.541	<i>a</i>	0.168	<i>a</i>	0.918	<i>b</i>
4101	H δ	+0.200	0.205	<i>c</i>	0.404	<i>b</i>	0.218	<i>a</i>	0.355	<i>b</i>
4340	H γ	+0.135	0.452	<i>b</i>	0.506	<i>a</i>	0.435	<i>a</i>	0.495	<i>b</i>
4363	[O III]	+0.130	0.075	<i>d</i>	0.138	<i>d</i>	0.014	<i>b</i>	0.268	<i>c</i>
4471	He I	+0.105	0.039	<i>a</i>
4686	He II	+0.045	0.056	<i>d</i>
4861	H β	0.000	1.000	<i>a</i>	1.000	<i>a</i>	1.000	<i>a</i>	1.000	<i>a</i>
4959	[O III]	-0.020	3.069	<i>a</i>	4.809	<i>a</i>	1.006	<i>a</i>	3.735	<i>a</i>
5007	[O III]	-0.030	9.381	<i>a</i>	14.621	<i>a</i>	3.353	<i>a</i>	11.154	<i>a</i>
5876	He I	-0.210	0.209	<i>d</i>	0.216	<i>c</i>	0.119	<i>a</i>
6548	[N II]	-0.330	0.307	<i>b</i>	0.120	<i>a</i>
6563	H α	-0.335	2.850	<i>a</i>	2.850	<i>a</i>	2.850	<i>a</i>	2.850	<i>b</i>
6583	[N II]	-0.340	0.578	<i>b</i>	0.820	<i>a</i>	0.356	<i>a</i>	0.334 ^b	<i>d</i>
6678	He I	-0.360	0.033	<i>b</i>
6717	[S II]	-0.370	0.134	<i>a</i>
6731	[S II]	-0.370	0.087	<i>a</i>
c			+0.365		+0.516		+0.455		+0.786	
$\log F(\text{H}\beta)$			-15.039		-15.213		-13.693		-15.461	
$\log I(\text{H}\beta)$			-14.674		-14.697		-13.238		-14.675	

^a Quality index is defined as: (a) 0%–5%, (b) 5%–10%, (c) 10%–20%, and (d) 20%–30% uncertainty.

^b Upper limit estimate.

TABLE 4
 DENSITY, TEMPERATURE AND IONIC CONCENTRATIONS

ION	M31-290		M31-363		BA 685	M31-372	
	Density (cm ⁻³) =		1000	10000	100	1000	10000
	10450	10280	11000	10820	8600	16040	15710
He ⁺	0.16	0.16	0.16	0.16	0.09
He ⁺⁺	0.01	0.01
O ⁺	2.92E-5	6.59E-5	4.10E-5	9.21E-5	1.38E-4	2.79E-6	6.09E-6
O ⁺⁺	2.66E-4	2.82E-4	3.54E-4	3.76E-4	1.84E-4	1.04E-4	1.10E-4
N ⁺	1.02E-5	1.20E-5	1.27E-5	1.49E-5	1.05E-5	<2.37E-6	<2.71E-6
Ne ⁺⁺	4.56E-5	4.86E-5	9.65E-5	1.03E-4	2.61E-5	2.75E-5	2.91E-5

$I(\lambda 3726)/I(\lambda 3729)$ and $I(\lambda 6717)/I(\lambda 6731)$. Our spectral resolution was too low to deconvolve the [O II] doublet, and the [S II] lines are too weak to be detected, except in the case of the H II region, where the line ratio indicates a density lower than 100 cm⁻³.

For the planetary nebulae, we must assume a density in order to derive abundances. We performed the analyses by adopting both 1000 cm⁻³ and 10,000 cm⁻³, values typical for luminous extragalactic planetary nebulae (Dufour and Killen 1977). Fortunately, none of the ionic concentrations considered here strongly depends on the density over this range.

The electron temperatures were calculated from the ratio of $I(\lambda 4363)$ to $I(\lambda 5007)$. The derived temperature is a very weak function of the electron density.

Ionic concentrations relative to hydrogen were calculated from the line ratios in Table 3, the density, and the temperature. We followed the procedures of Dufour and Talent (1980) in deriving the ionic abundances and the correction factors to account for unseen stages of ionization, but we assumed the nebulae are isothermal; that is, there are no temperature fluctuations. The derived ionic concentrations are listed in Table 4, and the elemental abundances are given in Table 5. These abundances supersede the preliminary values given by Ford (1983). For comparison we have also included in Table 5 abundances for Orion (Peimbert and Torres-Peimbert 1977), a typical Galactic planetary nebula (Aller and Czyzak 1983), a typical type I planetary nebula (Peimbert 1978), and the halo planetary nebulae K648 (in the globular cluster M15) and 49+88°1 (Hawley and Miller 1978). Even though M31-290 and M31-363 have relatively high helium abundances, it is clear from Table 5 that they differ from Galactic Type I planetaries, which are believed to be derived from Population I progenitors.

With the exception of the abundance of helium, the uncertainty in the derived abundances is dominated by the uncertainty in the electron temperature. The helium abundance is only slightly dependent on temperature, and so its uncertainty is primarily a function of the error in the measured line strength of He I $\lambda 5876$. For M31-290 and M31-363, the uncertainties are ~30% and ~15% while for the brighter H II region, BA 685, the uncertainty is under 5%.

Ionized helium was marginally detected in M31-290, where the line strength is ~5% of H β . This corresponds to an abundance of ionized helium relative to hydrogen of 0.005. This has a minor effect (+0.01 dex) on the ionization correction scheme used for the other elements.

The electron temperature is a strong function of the strength of the [O III] $\lambda 4363$ line. We estimate the uncertainty in this line for the three planetary nebulae to be 28%, 21%, and 19%

respectively, for radial distances of 3.5, 18, and 33 kpc. Despite the fact that the most distant planetary is the faintest, the uncertainty is the smallest because it received the most observation (6.7 hr) and its abundances are the lowest. The lack of coolants results in a high electron temperature, which is shown by the strong emission in 4363 Å. The H II region, although cool, is so much brighter than the planetaries that the uncertainty in $I(\lambda 4363)$ is ~8%.

We investigated the effect of decreasing $I(\lambda 4363)$ by 15% on the derived abundances for the 18 kpc planetary nebula. In summary, the logarithmic abundances for helium, oxygen, nitrogen, and neon respectively decrease by 0.004, 0.074, 0.036, and 0.092. In addition, strengths of important lines relative to H β have uncertainties on the order of 5%–15% depending on the strength of the line and the integration time. This translates to an additional error in the logarithmic abundance of ~0.04. Thus, typical uncertainties for the logarithmic abundance of helium, oxygen, nitrogen, and neon are respectively 0.09, 0.12, 0.09, and 0.12. Those for the H II region are considerably smaller.

Note that these uncertainties are based on the statistical errors in the observational measurements and do not include the uncertainties in the diagnostic technique, such as the use of ionization correction schemes and effects of temperature fluctuations and inhomogeneities which are averaged in the integrated spectra of the nebulae.

 TABLE 5
 ELEMENTAL ABUNDANCES

Object	$\left[12 + \log \left(\frac{N}{N_H} \right) \right]$				Reference
	He	O	N	Ne	
M31-290 ^a	11.20	8.55	7.81	7.79	
M31-363 ^a	11.21	8.67	7.88	8.11	
BA 685	10.93	8.51	7.39	7.66	
M31-372 ^a	8.06	<7.71	7.49	
Orion	11.00	8.52	7.57	7.66	1
NGC 1624	11.09	8.2	7.08	7.34	2
Galactic PNs	11.04	8.64	8.26	8.03	3
Type I PNs	11.20	8.8	9.0	8.2	4
49+88°1	11.03	8.34	7.80	6.72	5
K648	11.00	7.65	7.11	6.40	5

^a Abundances for a density of 10,000 cm⁻³.

REFERENCES.—(1) Peimbert and Torres-Peimbert 1977, assuming $\langle t^2 \rangle = 0.0$. (2) Talent and Dufour 1979. (3) Aller and Czyzak 1983. (4) Peimbert 1978. (5) Hawley and Miller 1978.

TABLE 6
H II TEMPERATURES IN M31
(K)

H II REGION	R (kpc)	MEASURED	PREDICTED		
			PEBCS	DK	BKC
BA 685.....	17	8600	8840	8550+500	7475+1100

IV. DISCUSSION

Comparison of planetary nebula abundances with abundances derived from H II regions and supernova remnants (SNRs) provides a way of measuring the enrichment of the interstellar medium subsequent to the formation of the planetary progenitors. Dennefeld and Kunth (1981, hereafter DK) and Blair, Kirshner, and Chevalier (1982, hereafter BKC) derived abundances for H II regions and SNRs across M31. Because of the difficulty of measuring the temperature diagnostic from the [O III] lines, $I(\lambda 4363)/I(\lambda 5007)$, in low-excitation H II regions, DK and BKC used the Pagel *et al.* (1979, hereafter PEBCS) empirical calibration of $[I(\lambda 3727) + I(\lambda 5007)]/H\beta$ versus mean temperature $\langle t \rangle$ to estimate the temperature in the H II regions. We can use our direct measurement of the temperature in the H II region BA 685 at $R = 17$ kpc to check the PEBCS calibration and the $\langle t \rangle$ versus R relations derived by DK and BKC. The measured and predicted temperatures are given in Table 6.

Table 6 shows that our measured temperature agrees quite well with the temperature predicted by the PEBCS calibration of $[I(\lambda 3727) + I(\lambda 5007)]/H\beta$ versus $\langle t \rangle$. Our temperature also validates the dependence of $\langle t \rangle$ versus R derived by DK and BKC. There is excellent agreement with the DK prediction at $R = 17$ kpc and reasonable agreement with the BKC scale. Likewise, there is satisfactory agreement between our derived oxygen abundance in BA 685, $O/H = 3.2 \times 10^{-4}$, and the predicted values, $O/H = 3.6 \pm 0.9 \times 10^{-4}$ (DK) and $O/H = 5.4 \pm 2.5 \times 10^{-4}$ (BKC). Similarly, for nitrogen, our derived abundance is $N/H = 2.5 \times 10^{-5}$, the predicted values, $N/H = 1.6 \pm 1.4 \times 10^{-5}$ (DK) and $NH = 2.7 \pm 1.5 \times 10^{-5}$ (BKC).

We first note that abundances in M31's interstellar medium at 17 kpc are high in comparison with the Galaxy. In spite of the fact that the present star formation rate in M31 is lower than in the Galaxy, and quite low at $R = 17$ kpc, where spiral arms are almost indiscernible (cf. Sandage 1961; Baade and Arp 1964), the abundances at 17 kpc are about the same as in the Orion nebula, whose galactocentric distance is 10 kpc (see Table 5). The Galactic abundances of nitrogen and oxygen in NGC 1624 (Talent and Dufour 1979) at $R = 14$ kpc are much lower than in M31 at 17 kpc. There can be little doubt that

M31 experienced considerably more enrichment of its interstellar medium during its early life than did the Galaxy.

Before discussing the planetary abundances, we first consider what can be said about their parent populations based on the observed radial velocities. Nolthenius (1984) and Nolthenius and Ford (1986) have analyzed the radial velocities of 34 planetary nebulae in the outer disk and halo of M31. The analysis shows that the majority of nebulae with projected radii less than 30 kpc belong to a thick disk population ($\langle z \rangle = 3$ kpc) with a dispersion of 39 km s^{-1} in the θ -direction about a flat rotation curve. By comparison with type II planetaries in the Galaxy (Peimbert 1978), which have $\langle z \rangle = 150$ pc and respective progenitor masses and ages of approximately $1.5 M_{\odot}$ and 2×10^9 yr, we conclude that the nebulae in M31's outer disk derive from stars with ages of at least 2×10^9 yr. Because of the relatively low rate of star formation in M31 at distances greater than 20 kpc, it is likely that the planetary progenitors in the thick disk are in fact considerably older than this. We note that the thick disk could be attributed to a low density of material in the outer disk. The H I dispersion ($\langle z \rangle \approx 1$ kpc; Emerson 1978) indicates that this effect may be present, but not dominant.

In addition to the distant disk population of planetaries, which follow M31's rotation curve, there is a conspicuous group of planetaries which derive from a halo population. Excluding planetaries in the center of M31 (Lawrie and Ford 1982; Lawrie 1983), we have measured radial velocities for 52 nebulae. Seven of these would have high velocities as seen from M31's disk, which shows their kinship with M31's halo population of globular clusters. Huchra, Stauffer, and van Speybroeck (1982, hereafter HSvS) extended van den Bergh's (1969, hereafter SvdB) kinematical and metallicity studies of 40 clusters to a total of 70 clusters. Inspection of their plot of cluster radial velocities versus distance from the minor axis shows that $\sim 35\%$ of the clusters have high-velocity orbits. These orbits show that the globular cluster system is slowly rotating with an azimuthal velocity dispersion which is large compared to the rotation velocity. The planetary nebulae in high-velocity orbits almost certainly have their origin in the same population as the globular clusters, or one that is closely related to it.

The kinematical properties of our three nebulae and the H II region BA 685 are summarized in Table 7. The nebular coordinates X and Y are relative to an assumed major axis at P.A. = 38° (Baade and Arp 1964), and the predicted radial velocities are derived from a projection onto Rubin and Ford's (1970) rotation curve for M31 assuming an inclination of 77° . Although M31-290 was chosen in order to sample the disk population at 3.5 kpc, and thus provide a long baseline for measuring an abundance gradient in the disk, by bad luck the nebula has a radial velocity of -660 km s^{-1} . This velocity, which is approximately 500 km s^{-1} more negative than the

TABLE 7
KINEMATIC PROPERTIES OF NEBULAE IN M31

Nebula	X	Y	$R_{\text{projected}}$ (kpc)	$V_{\text{predicted}}$ (km s^{-1})	V_{observed} (km s^{-1})	Population
M31-290.....	17.86	-1.45	3.5	-129	-660	Halo
M31-363.....	93.57	-13.67	18.4	-139	-94	Disk
BA 685.....	84.46	-8.60	16.6	-116	-92	Disk
M31-372.....	154.92	-66.98	32.9	-98	-110	Halo

velocity predicted from M31's rotation curve at its projected position, shows that it is in a high-velocity orbit, and thus, by the previous arguments, is a member of the halo. Because of its high velocity, it is unlikely that M31-290 can be associated with the disk population at $R = 3.5$ kpc.

The planetary M31-363 at $R = 18$ kpc has a radial velocity close to that of the rotation curve defined by the other planetaries (the planetary rotation curve is flat and in agreement with the optical and H I rotation curves) and almost certainly is a member of the old disk population at its projected position. The planetary M31-372 at $R_{\text{projected}} = 33$ kpc also has a radial velocity near the value predicted at its apparent position from a disk with a flat rotation curve. However, we think it is unlikely that this nebula is a member of a disk population. If it is in an undistorted disk with $i = 77^\circ$, its projected distance rectifies to a true radial distance of 65 kpc, and the implied circular velocity of the disk is approximately 400 km s^{-1} relative to M31. If we use the bent disk model of Newton and Emerson (1977), in which the inclination of the outer disk increases to 83° , the rectified distance becomes 79 kpc and the implied circular velocity is 500 km s^{-1} . In either case the circular velocity is implausibly large, and the nebula would be at such a large distance that we would be improbably fortunate to have found it, given the observed number of nebulae per unit luminosity in the bulge (Ford and Jacoby 1978*b*) and disk at $R = 20$ kpc (Nolthenius and Ford 1986). Consequently, we conclude that it is a member of M31's halo population. This assignment is consistent with classifications in the Galaxy; any object with a minimum distance of 20 kpc or greater would almost certainly be presumed to belong to the Galaxy's halo.

Comparison of abundances in planetary nebulae and H II regions is complicated by the fact that CNO burning in the planetary progenitor changes its original composition. However, Renzini and Voli (1981) used stellar models to conclude that, unlike carbon and nitrogen, "all in all the envelope oxygen abundance suffers only minor variations, contrary to the case of the other CNO isotopes." This conclusion is substantiated by the fact that the variations in O/H are relatively small between classes of planetaries which have different progenitor masses and which show large variations in N/O (Aller 1983; Peimbert and Torres-Peimbert 1983; Kaler 1983). Consequently, the fact that the oxygen abundance in the planetary M31-363 and the H II region BA 685 are equal within their mutual uncertainties shows that the old stars in the outer disk at $R = 18$ kpc share the high abundance of the residual gas, which has abundances equal to the Orion nebula at $R = 10$ kpc in the Galaxy. This indicates that the epoch of enrichment occurred before the birth of the planetary progenitors, a time which we infer to be considerably greater than 2×10^9 yr ago, and shows that there has been little, if any, enrichment of the remote disk since their birth. The relative high abundance of nitrogen in M31-363 reflects the well-established fact that planetaries produce nitrogen through CNO burning (Renzini and Voli 1981; Peimbert and Torres-Peimbert 1983). Although the planetary nebula birth rate and star formation rate are too poorly known at this large distance in M31 to use Tinsley's (1978) criterion to see if the planetaries presently are a significant source of nitrogen enrichment for the disk gas, we speculate that this is the case, as is likely in the solar neighborhood (Tinsley 1978).

Comparison of the oxygen abundances in the two halo planetaries M31-290 ($R_{\text{projected}} = 3.5$ kpc) and M31-372 ($R_{\text{projected}} = 33$ kpc) provides direct additional evidence for the chemical inhomogeneity in M31's halo found from measure-

ments of the integrated line strengths of globular clusters (SvdB; HSvS). The oxygen abundance in M31-290 is equal to that of Orion and old Galactic disk planetaries, whereas the abundances in M31-372 are intermediate between the Galactic Population II halo planetary 49+88°1 (Hawley and Miller 1978) and the Galactic halo planetary K648 in the extremely metal-poor Population II globular cluster M15 (see Table 5). The abundances in M31-372 support our classifying it as a member of M31's halo and provide a direct measurement of the chemical composition in the metal-poor component of M31's halo.

It is curious that the helium abundances of the M31 halo planetary nebulae are a factor of 1.5 higher than those of Galactic halo planetary nebulae. Furthermore, the neon to oxygen ratio is about 7 times higher than in the halo planetary nebulae listed in Table 5. Note, however, that the Galactic halo planetary nebula 108-76°1 has a neon to oxygen ratio similar to those of the M31 planetary nebulae (Hawley and Miller 1978) and a nitrogen to oxygen ratio about 10 times greater. As for the helium abundance, we reiterate that the helium lines are weak, although the disparity is larger than we expect from observational uncertainty alone. Perhaps there exists a considerable range in the abundances of halo planetary nebulae.

SvdB and HSvS found both weak-line and strong-line clusters at large distances from the center of M31 and a relatively weak gradient of line strengths. The mixing of weak-line and strong-line clusters in M31's halo can be illustrated in another way. We used HSvS's data to compute the mean and standard deviations of the line strength indicator $\langle \text{Ca II K} \rangle$, which varies from 6.9 to 16.7, for 42 "prograde" clusters and 20 high-velocity clusters, obtaining $\langle \text{Ca II K} \rangle_{\text{prograde}} = 11.64 \pm 2.27$ and $\langle \text{Ca II K} \rangle_{\text{high-velocity}} = 11.87 \pm 2.06$. The mean metallicities and the dispersions about the means are indistinguishable. As further evidence of the compositional and kinematical heterogeneity in M31's halo, we note that the cluster with the strongest $\langle \text{Ca II K} \rangle$ line strength indicator, B39 (Battistini *et al.* 1980), is in a high-velocity orbit, and the ("prograde") cluster with the highest radial velocity (B201, $v_r = -701 \text{ km s}^{-1}$, $R_{\text{projected}} = 2.8$ kpc) has a line strength index $\langle \text{Ca II K} \rangle = 12.1$, which is higher than the mean. The planetary M31-290 ($v_r = -660 \text{ km s}^{-1}$, $R_{\text{projected}} = 3.4$ kpc) with its relatively high oxygen abundance appears to be a stellar counterpart to B201.

The preceding considerations show that there is little, if any, evidence in the radial velocities of M31's globular clusters for a kinematical metallicity dependence. This differs from the Galaxy, where Pier's (1984) solutions for the solar motions of the metal-poor and metal-rich clusters show that the latter may be rotating much faster than the former. The only evidence for a kinematical metallicity dependence in M31 is the weak metallicity gradient seen by HSvS, reflecting the fact that, as in the Galaxy (Smith 1984), there appears to be a metal-rich tail on the distribution of metallicities in the inner halo. Apart from this, the evidence suggests that a wide range of metal enrichment occurred during the collapse of M31's halo, with little progressive enrichment toward the center. Further clarification of the kinematical and chemical history of M31's disk and halo will require additional work on planetary nebulae in M31.

We wish to thank Richard Nolthenius for calculating the kinematical properties of M31-372 in Newton and Emerson's bent disk model.

REFERENCES

- Aller, L. H. 1983, in *IAU Symposium 103, Planetary Nebulae*, ed. D. R. Flower (Dordrecht: Reidel), p. 1.
- Aller, L. H., and Czyzak, S. J. 1983, *Ap. J. Suppl.*, **51**, 211.
- Aller, L. H., Keyes, C. D., Ross, J. E., and O'Mara, B. J. 1981, *M.N.R.A.S.*, **194**, 613.
- Baade, W., and Arp, H. 1964, *Ap. J.*, **139**, 1027.
- Battistini, P., Bonoli, F., Braccisi, A., Fusi Pecci, F., Malagani, M. L., and Morano, B. 1980, *Astr. Ap. Suppl.*, **42**, 357.
- Blair, W. P., Kirshner, R. P., and Chevalier, R. A. 1981, *Ap. J.*, **247**, 879.
- . 1982, *Ap. J.*, **254**, 50 (BKC).
- Brocklehurst, M. 1971, *M.N.R.A.S.*, **153**, 471.
- Danziger, I. J., Dopita, M. A., Hawardin, T. G., and Webster, B. L. 1978, *Ap. J.*, **220**, 458.
- Dennefeld, M., and Kunth, D. 1981, *A.J.*, **86**, 989 (DK).
- Dufour, R. J., and Killen, R. M. 1977, *Ap. J.*, **211**, 68.
- Dufour, R. J., and Talent, D. L. 1980, *Ap. J.*, **235**, 22.
- Emerson, D. T. 1978, in *IAU Symposium 77, Structure and Properties of Nearby Galaxies*, ed. E. M. Berkhuijen and R. Wielebinski (Dordrecht: Reidel), p. 180.
- Ford, H. C. 1983, in *IAU Symposium 103, Planetary Nebulae*, ed. D. R. Flower (Dordrecht: Reidel), p. 443.
- Ford, H. C., and Jacoby, G. H. 1978a, *Ap. J. Suppl.*, **38**, 351.
- . 1978b, *Ap. J.*, **219**, 437.
- Goad, L. E. 1979, *Proc. SPIE*, **172**, 86.
- Hawley, S. A., and Miller, 1978, *Ap. J.*, **220**, 609.
- Huchra, J., Stauffer, J., and van Speybroeck, L. 1982, *Ap. J. (Letters)*, **259**, L57 (HSvS).
- Innanen, K. A., Kamper, K. W., Papp, K. A., and van den Bergh, S. 1982, *Ap. J.*, **254**, 515.
- Jacoby, G. H., and Lesser, M. P. 1981, *A. J.*, **86**, 185.
- Jenner, D. C., and Ford, H. C. 1978, in *IAU Symposium 76, Planetary Nebulae Observations and Theory*, ed. Y. Terzian (Dordrecht: Reidel), p. 246.
- Jenner, D. C., Ford, H. C., and Jacoby, G. H. 1979, *Ap. J.*, **227**, 391.
- Kaler, J. B. 1983, in *IAU Symposium 103, Planetary Nebulae*, ed. D. R. Flower (Dordrecht: Reidel), p. 245.
- Lawrie, D. G. 1983, *Ap. J.*, **273**, 562.
- Lawrie, D. G., and Ford, H. C. 1982, *Ap. J.*, **256**, 112.
- McClure, R. D., and Racine, R. 1969, *A. J.*, **74**, 1000.
- Newton, K., and Emerson, D. T. 1977, *M.N.R.A.S.*, **181**, 573.
- Nolthenius, R. 1984, Ph.D. thesis, University of California, Los Angeles.
- Nolthenius, R., and Ford, H.C. 1986, *Ap. J.*, submitted.
- Osmer, P. S. 1976, *Ap. J.*, **203**, 352.
- Pagel, B. E. J., Edmunds, M. G., Blackwell, D. E., Chun, M. S., and Smith, G. 1979, *M.N.R.A.S.*, **189**, 95 (PEBCS).
- Peimbert, M. 1978, in *IAU Symposium 76, Planetary Nebulae Observations and Theory*, ed. Y. Terzian (Dordrecht: Reidel), p. 215.
- Peimbert, M., and Torres-Peimbert, S. 1977, *M.N.R.A.S.*, **179**, 217.
- . 1983, in *IAU Symposium 103, Planetary Nebulae*, ed. D. R. Flower (Dordrecht: Reidel), p. 233.
- Pier, J. R. 1984, *Ap. J.*, **281**, 260.
- Renzini, A., and Voli, M. 1981, *Astr. Ap.*, **94**, 175.
- Rubin, V. C., and Ford, W. K. 1970, *Ap. J.*, **159**, 379.
- Sandage, A. 1961, *The Hubble Atlas of Galaxies* (Washington: Carnegie Institution of Washington).
- Smith, H. A. 1984, *Ap. J.*, **281**, 148.
- Talent, D. L., and Dufour, R. J. 1979, *Ap. J.*, **233**, 888.
- Tinsley, B. 1978, in *IAU Symposium 76, Planetary Nebulae Observations and Theory*, ed. Y. Terzian (Dordrecht: Reidel), p. 341.
- van den Bergh, S. 1969, *Ap. J. Suppl.*, **19**, 145 (SvdB).
- Whitford, A. E. 1958, *A.J.*, **63**, 201.

HOLLAND FORD: Space Telescope Science Institute, Homewood Campus, Baltimore, MD 21218

GEORGE JACOBY: Kitt Peak National Observatory, P.O. Box 26732, Tucson AZ 85726